

Review

Longwall Mining Automation—The Shearer Positioning Methods between the Longwall Automation Steering Committee and China University of Mining and Technology

Weiwei Dai ¹, Shijia Wang ^{2,*}  and Shibo Wang ¹

¹ School of Mechanical and Electronic Engineering, China University of Mining and Technology, Xuzhou 221116, China; d18649519857@163.com (W.D.); wangshb@cumt.edu.cn (S.W.)

² School of Mechanical Engineering, Yanshan University, Qinhuangdao 066004, China

* Correspondence: sjwang@ysu.edu.cn

Abstract: The shearer positioning method is of great significance to the automation of longwall mining. The research teams in the Longwall Automation Steering Committee (LASC) of Australia and China University of Mining and Technology (CUMT) have focused on shearer positioning and identified the shearer inertial navigation system, the measurement of longwall retreat and creep displacement, and the backward calibration of the shearer trajectory as three key technologies to obtain accurate shearer positioning information. In underground environments without GPS, due to the characteristics of inertial navigation system (INS) autonomous full-parameter navigation, shearer positioning based on INS is adopted by the LASC and CUMT, and error reduction algorithms are proposed to inhibit the rapid error accumulation of INS. In order to obtain the periodic calibration information when the shearer reaches the end of the longwall face, it is necessary to measure the retreat and creep displacements in order to back-correct the shearer trajectory. Finding a suitable measurement method for this task is challenging, especially in the presence of dust and moisture. The LASC used a scanning laser and FMR 250 microwave radar to measure these two displacements, while CUMT adopted an ultra-wideband (UWB) radar. In terms of the backward calibration method, minimum-variance fixed-interval smoothing (MFS) proposed by LASC and the global optimization model (GOM) for the shearer trajectory from CUMT are described in detail. The experiment demonstrates that the GOM outperforms MFS in terms of accuracy but requires more computational resources. Therefore, our next research objective is to develop an efficient and accurate algorithm for performing backward calibration on the shearer trajectory.

Keywords: shearer positioning; longwall mining automation; inertial navigation system; longwall retreat and creep displacement measurement; backward calibration



Citation: Dai, W.; Wang, S.; Wang, S. Longwall Mining Automation—The Shearer Positioning Methods between the Longwall Automation Steering Committee and China University of Mining and Technology. *Appl. Sci.* **2023**, *13*, 12168. <https://doi.org/10.3390/app132212168>

Academic Editor: Lina M. López

Received: 30 August 2023

Revised: 24 October 2023

Accepted: 26 October 2023

Published: 9 November 2023



Copyright: © 2023 by the authors. Licensee MDPI, Basel, Switzerland. This article is an open access article distributed under the terms and conditions of the Creative Commons Attribution (CC BY) license (<https://creativecommons.org/licenses/by/4.0/>).

1. Introduction

Longwall mining is a primary method for extracting coal from underground mines. As shown in Figure 1, three kinds of mining equipment used in the longwall face are a shearer, an armored face conveyor (AFC), and a roof support system. The shearer moves back and forth along a rail connected to the AFC, while the roof support system maintains the stability of the coal seam roof. Traditionally, the shearer and roof support system are controlled manually, which inevitably causes the rock to contaminate the coal and reduces the mining productivity. In addition, worker safety is greatly threatened because they are directly exposed to the mining worksite. Improving mining productivity, protecting worker safety, and achieving environmental sustainability are the goals that the coal mining industry has been pursuing [1,2]. Longwall mining automation is a mining process that is carried out using mining equipment without the need for manual intervention. It involves the intelligent perception of the mining environment, intelligent control of the mining equipment, and autonomous operation of the mining process [3,4]. Longwall

mining automation technology has shown significant potential to achieve those goals through providing shearer positioning, face alignment, horizontal control, seam tracking, visualization and monitoring, and remote control [5,6]. Among them, shearer positioning is a foundational aspect of the autonomous mining operation, and it is a key technology that enables face alignment and horizontal control. Therefore, the accurate positioning of the shearer is of great significance to longwall mining automation.

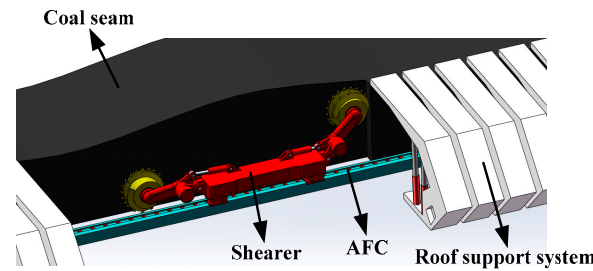


Figure 1. The diagram of the shearer, AFC, and roof support system.

As early as 2001, the Commonwealth Scientific and Industrial Research Organization (CSIRO) of Australia began developing the longwall automation technology known as the Longwall Automation Steering Committee (LASC). LASC is the abbreviation for the research team responsible for this technology. The LASC can fix the 3D position of the shearer, maintain the straightness of the conveyor and supports, raise the shearer drum automatically, and provide 3D remote monitoring video feeds [7–9]. The technical framework is shown in Figure 2b. The latest version, LASC 2.0, has been adopted in 70% of Australia’s coal mines. DBT, JOY, and Eickhoff are all licensed manufacturers of LASC. The social benefits of LASC application have contributed to reducing the number of accidents and deaths, and the costs that are avoided as a result are likely to save mining industries millions of dollars each year. In addition, improving the accuracy of longwall mining operations and reducing the amount of waste rock leads to less environmental disruption. LASC technology has great influence on the development of longwall mining automation around the world.

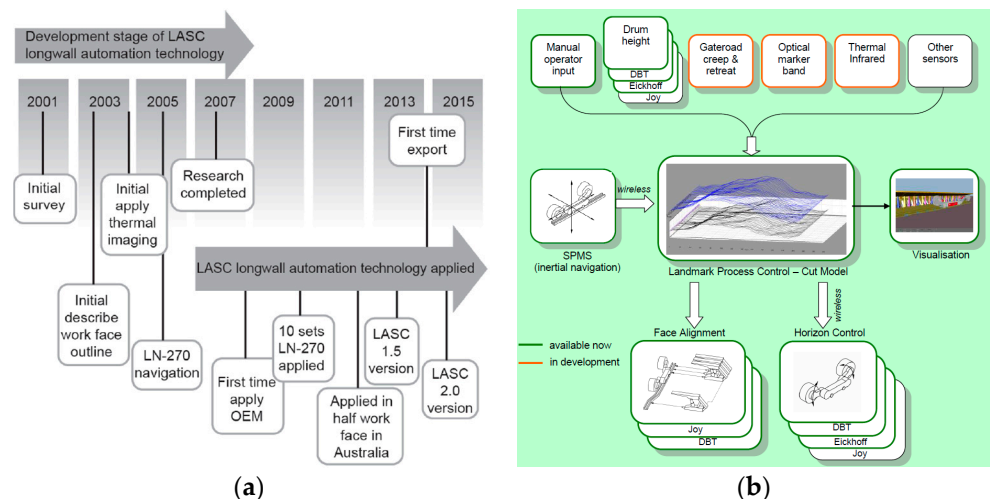


Figure 2. The diagram of (a) the development stage of LASC [6] and (b) the technical framework of LASC.

In China, research on the automation of longwall mining commenced at a relatively later stage. Under the support of the National High-tech Research and Development Program (863 Program) and the National Natural Science Foundation of China, our research group at China University of Mining and Technology (CUMT) has devoted significant

efforts to the longwall mining automation. Figure 3 shows the technical framework developed by CUMT for this purpose. The digital model of a coal seam is constructed using drill geological data and the seismic CT detection technique. Combining the digital model of the coal seam, shearer positioning technology is employed to obtain the shearer 3D positioning within the coal seam [10]. Based on this, it is possible to achieve AFC trajectory straightening and shearer cutting path planning. The industrial test was carried out and demonstrated satisfactory performance.

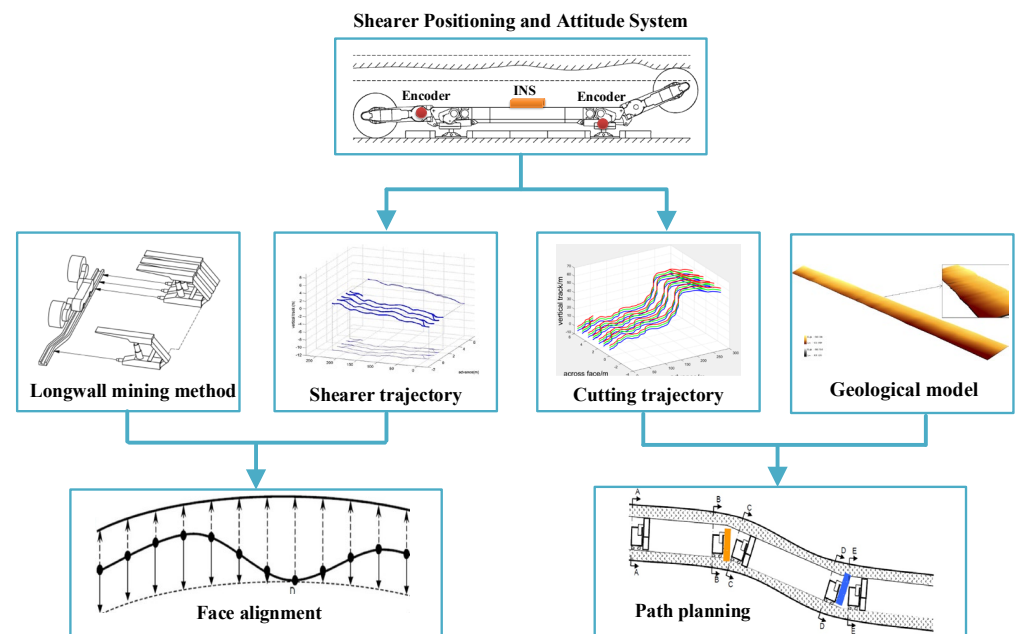


Figure 3. The technical framework of CUMT.

Whether it is for LASC or CUMT, the shearer positioning method plays an important role in longwall mining automation. The shearer inertial navigation system, the measurement of longwall retreat and creep displacement, and the backward calibration of shearer trajectory are three crucial technologies to acquire the shearer's accurate positioning. Therefore, this paper aims to present an overview of three technologies utilized by the LASC and CUMT, and compares the backward calibration methods proposed by the LASC and CUMT through a conducted experiment.

2. Longwall Mining Method

Longwall mining is widely recognized as a highly efficient method for extracting coal from underground mines. In a coal seam, many elongated and narrow roadways are excavated to form the boundaries of several longwall panels, as shown in Figure 4a. The roadways serve as a passageway of transportation for coal, equipment, and workers. The sectional area of roadway is approximately 5×4 m in general. The coal is extracted from the longwall panel, which is generally 300 min wide and 5000 min long, with a thickness ranging from 1.2 to 8.0 m. At the end of the longwall panel, the shearer, AFC, and roof support system are installed across the longwall face.

As shown in Figures 4b and 5, the shearer moves along a rail associated with the AFC, cutting a 0.8 m-wide slice of coal from the coal seam. The extracted coal is deposited onto the AFC and subsequently transported far away the longwall face. When the shearer is in motion, the hydraulic push arms, which are connected to the roof support system, gradually push a section of the AFC behind the shearer along the advancing direction for the next cutting cycle. In Figure 6, the shearer is in operation during n -th cycle, while the AFC behind the shearer has been moved into the $n + 1$ cycle. When the coal is cut, the roof support systems support the roof of the coal seam. There are approximately 200 roof

support systems in a typical longwall face. After the AFC is pushed towards the coal seam, the roof support systems are relocated along the advancing direction. Behind the roof support systems, the collapse of the roof results in the formation of a goaf.

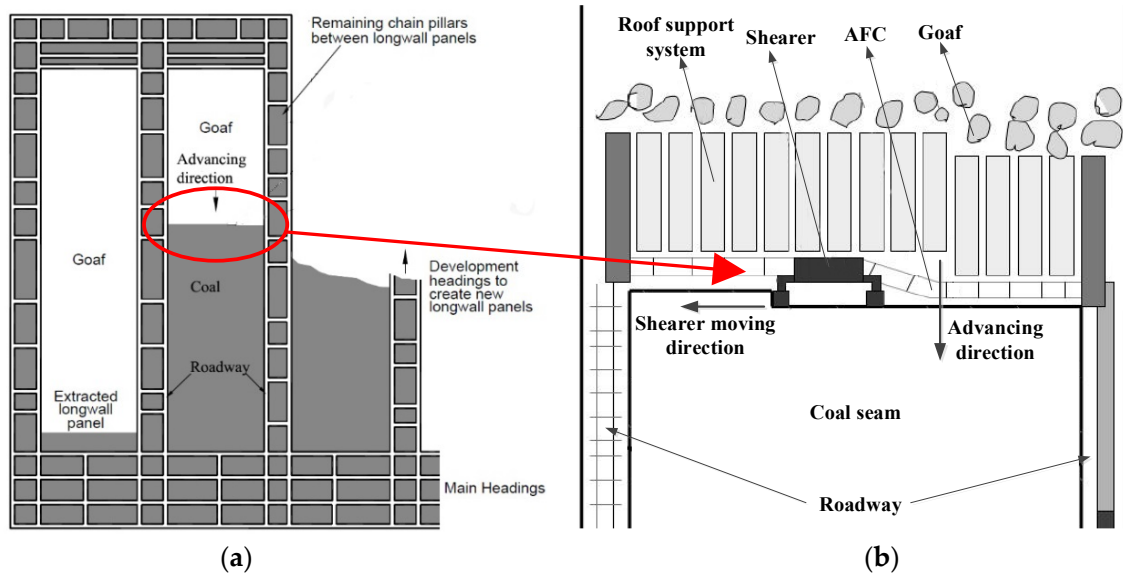


Figure 4. Typical plan view of (a) a coal mine and (b) a longwall face [11].



Figure 5. The shearer, AFC, and roof support system across the longwall face in an underground mine.

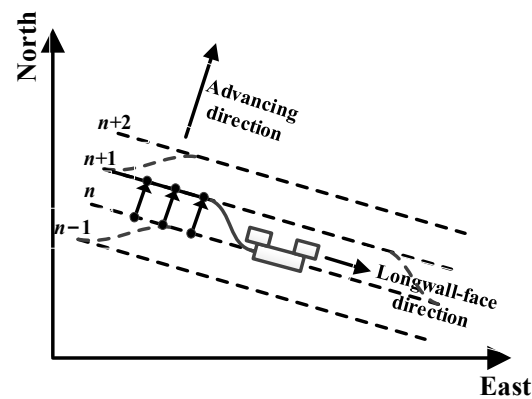


Figure 6. The diagram of the AFC profile as the shearer moves.

3. Shearer Positioning Technology

The shearer positioning method includes three components, the shearer inertial navigation system, the measurement of longwall retreat and creep displacements, and the backward calibration of the shearer trajectory. Researchers in the LASC and CUMT have been focusing on those three aspects and have acquired good results.

3.1. The Shearer Inertial Navigation System

Due to the unavailability of Global Position System (GPS) and BeiDou Navigation Satellite System (BDS) signals in underground environments, the positioning method based on the inertial navigation system (INS) is considered to be a feasible shearer positioning method. The INS exhibits a high level of autonomy, making it widely applied in aircraft [12], ships [13], submarines [14], and so on. The accelerometer and gyroscope serve as the core measurement units to obtain the state of an object. The tri-axis accelerometer measures the linear accelerations of an object with respect to its body reference frame in three orthogonal axes. The gyroscopes are utilized to quantify the angular velocities of rotation of the object with respect to the inertial reference frame. In summary, the navigation algorithm of the INS is founded upon the principles of Newton's laws of motion. The attitude angles are derived through the integration of rotational angular velocities. Subsequently, the rotation matrix, also known as the direction cosine matrix (DCM), is obtained. Through integrating the measured accelerations from the accelerometers and applying the rotation matrix transformation, the velocity and position in the navigation coordinate frame can be determined [15,16].

In order to acquire the shearer position in three dimensions (3D), the LASC has developed a measurement system known as the Shearer Position Measurement System (SPMS). This system utilizes a Northrop Grumman LN270 INS, as shown in Figure 7a. The LN270 was installed within an explosion-proof enclosure in the shearer body. In addition to the INS, an odometer, connected to the shearer haulage unit, was required to accurately measure the distance traveled across the longwall face. Afterwards, the second-generation SPMS (SPMS-II) using IXSEA PHINS INS was finished, as shown in Figure 7b. Due to the noise and vibration in underground environments, the INS calculation error increases exponentially over time. That is to say, the INS exhibits a very low relative error over short time periods, but over long time periods, the error increases dramatically. Based on this, Reid et al. [17] employed zero-velocity updating technology (ZUPT) to periodically correct the velocity error during stationary motion for an INS. Furthermore, the development of integrated navigation with an INS and odometer aims to continually enhance performance. After replacing the odometer with a Doppler radar, Dunn et al. [18,19] introduced a practical and accurate aiding source. Through analyzing the longwall mining method, Reid et al. [20] determined that the horizontal closing distance between two adjacent cutting cycles remained constant. This constant value was found to be instrumental in enhancing the longtime stability of the INS. The 3D path of a shearer in an underground mine, measured using the SPMS, is shown in Figure 8.

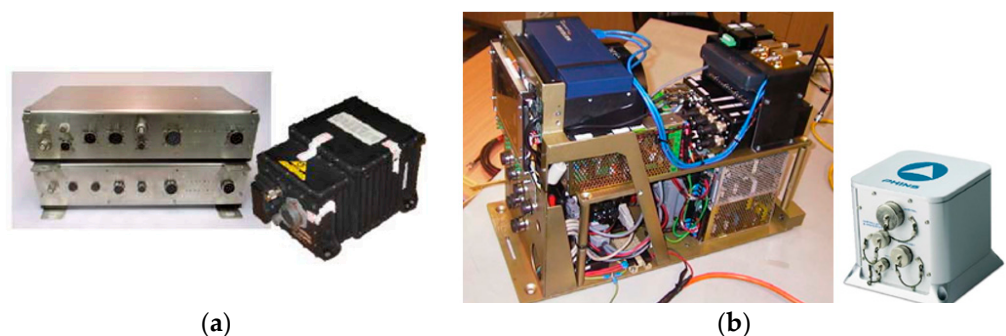


Figure 7. The shearer position measurement system (SPMS): (a) SPMS-I and (b) SPMS-II [17–19].

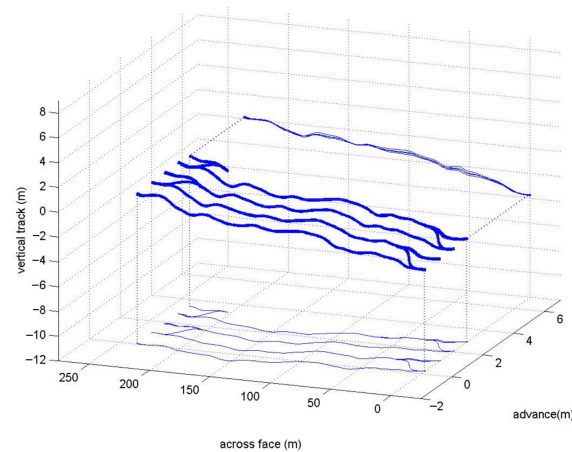
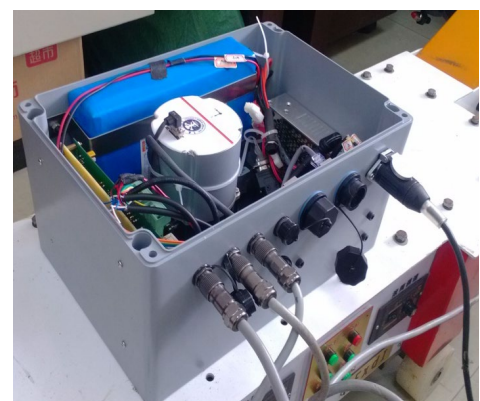


Figure 8. The shearer's 3D path in an underground mine measured using the SPMS [21].

In CUMT, the authors of this paper built the Shearer Positioning and Attitude Systems (SPAS), including SPAS-I and SPAS-II, as shown in Figure 9. The Spatial FOG INS from ADVANCED NAVIGATION provided the attitude angles of heading, pitch, and roll. The axial encoder connected to the travelling unit provided the velocity value of the shearer. The shearer position was then obtained using the dead-reckoning algorithm. The effect of the installation and initial alignment noncoincidence of the INS on the shearer positioning error was analyzed, and a calibration method for the two deviation angles with the two-point method was proposed [22,23]. The current axial encoder is a 12-bit system with a resolution of $1/4096$. This implies that the accuracy of INS attitude greatly affects the position error, especially the heading angle accuracy. Based on previous research, the heading angle error was found to increase at a faster rate than the pitch error and roll error over time. Furthermore, it was observed that the heading angle error directly affected the plane positioning accuracy [24,25]. According to the longwall mining method, two constraints on the shearer velocity and position were obtained. Therefore, the dynamic zero velocity update (DZUPT) model [26] and the closing path optimal estimation model [27] were built using a Kalman filter. In order to improve shearer positioning accuracy, an information filter was proposed to integrate these two models [11]. An underground field test was performed at 18,201 longwall faces in Shanxi Province, China, and Figure 10b shows the shearer trajectory acquired via the SPAS.



(a)



(b)

Figure 9. The shearer positioning and attitude system (SPAS): (a) SPAS-I and (b) SPAS-II.

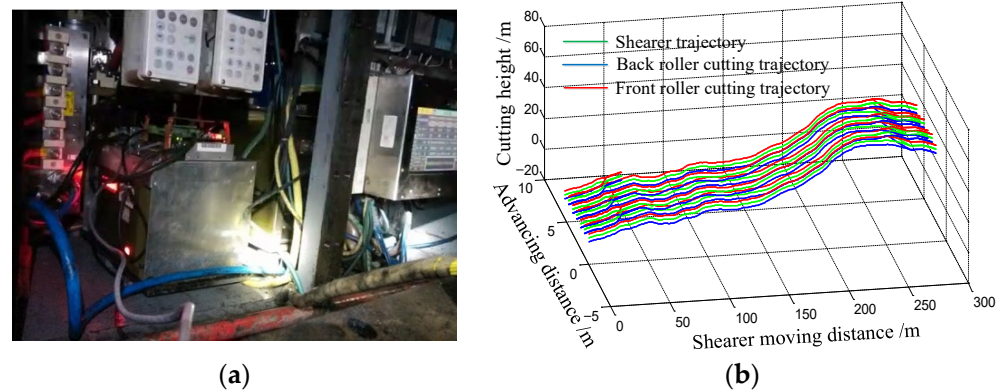


Figure 10. The diagram of (a) the underground field test in Shanxi and (b) the shearer trajectory acquired using the SPAS [28].

3.2. The Measurement Method of Longwall Retreat and Creep Displacements

In Section 3.1, the utilization of auxiliary sensors, ZUPT, DZUPT, and kinematics model reduced INS drift error and improved the positioning accuracy. However, due to the lack of periodic GPS calibration, the INS longtime error is still relatively large. After several cutting cycles, the shearer positioning accuracy cannot meet the requirement of the longwall mining automation. According to the longwall mining method, the shearer reciprocates between two roadways along the longwall face. When the shearer reaches the end of the longwall face, the longwall retreat and creep displacements become significant parameters to measure, which can be utilized to back-correct the shearer trajectory after the completion of each cutting cycle. As shown in Figure 11, according to the longwall mining method, the retreat displacement is actually the advancing distance of the mining equipment along the advancing direction every time. Due to the different levels of inclination of the longwall face, there will be a height difference between the two ends of the longwall face. When the mining equipment is installed on the inclined longwall face, the force acting on the equipment is not balanced, which makes the equipment slide along the longwall-face direction and produces the displacement of sliding up and down.

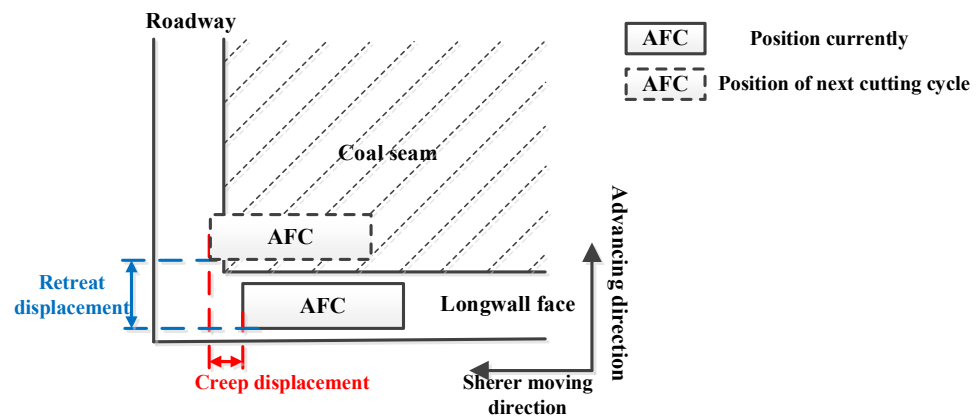


Figure 11. The diagram of the longwall retreat and creep displacements.

In the LASC, Reid et al. [20] installed the scanning laser on the roadway conveyor structure linked to the AFC to scan the roadway profile. Accordingly, the first generation of a scanning device with SICK LMS200 as the core sensor and the second generation of an explosion-proof 3D laser scanning device called ExScan have been developed. The current scan was matched to the global map with the scan-matching algorithm to acquire the retreat and creep displacements, as shown in Figure 12. However, the dust and moisture in an underground mine would greatly increase the attenuation and distortion of the laser beam, which affect the laser measurement accuracy. Then, Hargrave et al. [29–31] used

the FMR 250 radar from Endress-Hauser company in Germany to measure the retreat and creep displacements, and a field test in Australia's Beltana mine was carried out to verify the effectiveness of the proposed method, as shown in Figure 13. The radar is sensitive to distance information, and the creep displacement was obtained through measuring the distance between the radar and roadway wall. The number of bolt-plates on the roadway surface represented the position information, thus enabling the measurement of retreat displacement through the recognition of these bolt-plates. However, in the majority of mines, the bolt-plates lack position information, thereby limiting the applicability of this method.

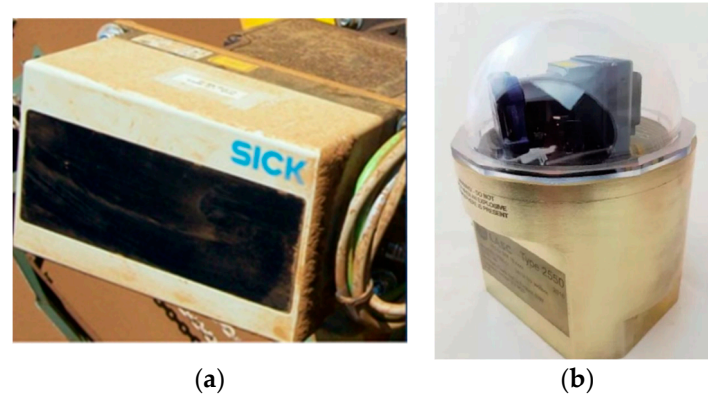


Figure 12. The diagram of (a) the SICK LMS200 scanning laser and (b) ExScan.

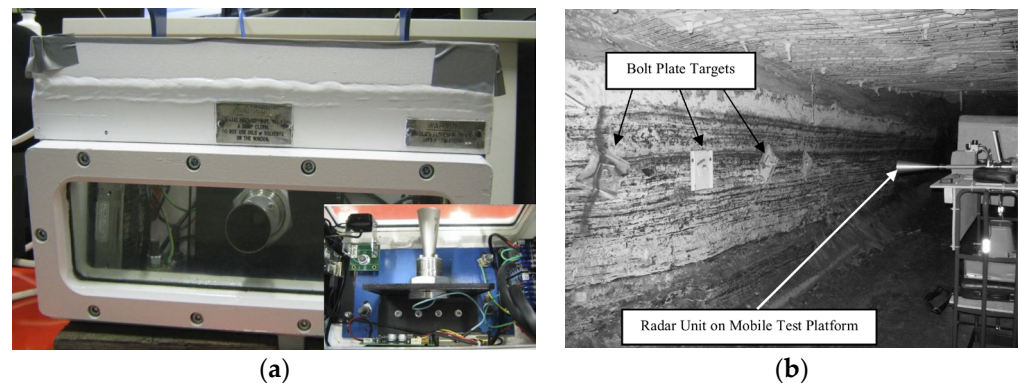


Figure 13. The diagram of (a) the Endress-Hauser FMR 250 radar and the (b) field test in an underground mine [29–31].

In CUMT, the authors of this paper provided a novel measurement solution with the ultra-wideband (UWB) radar imaging method [32]. UWB radar is characterized by a radar with a fractional bandwidth exceeding 25%. Through transmitting electromagnetic wave signals with a strong ability to penetrate a coal-dust environment, UWB radar can obtain target or scene images all day and in all weather, which has the technical advantage of application in the complex environment at the end of a longwall face. As shown in Figure 14a, the radar was mounted on a slide-way, and the slide-way was placed on the roadway conveyor structure connected to the head of the AFC. The radar was moved along the slide-way to image the bolt-plates. Two imaging results were obtained before and after the movement of the longwall face. Then, the feature-based image registration algorithm was employed to identify the correct-match pairs, and subsequently, the similarity transformation model was calculated to determine the retreat and creep displacements. The measurement device was developed (Figure 14b), and the algorithm program including radar imaging and image registration were embedded. The field text was performed in Xuzhuang Coal, China National Coal Group Corporation, and the mean values of retreat and creep measurement displacements were 8.0 mm and 8.6 mm, respectively.

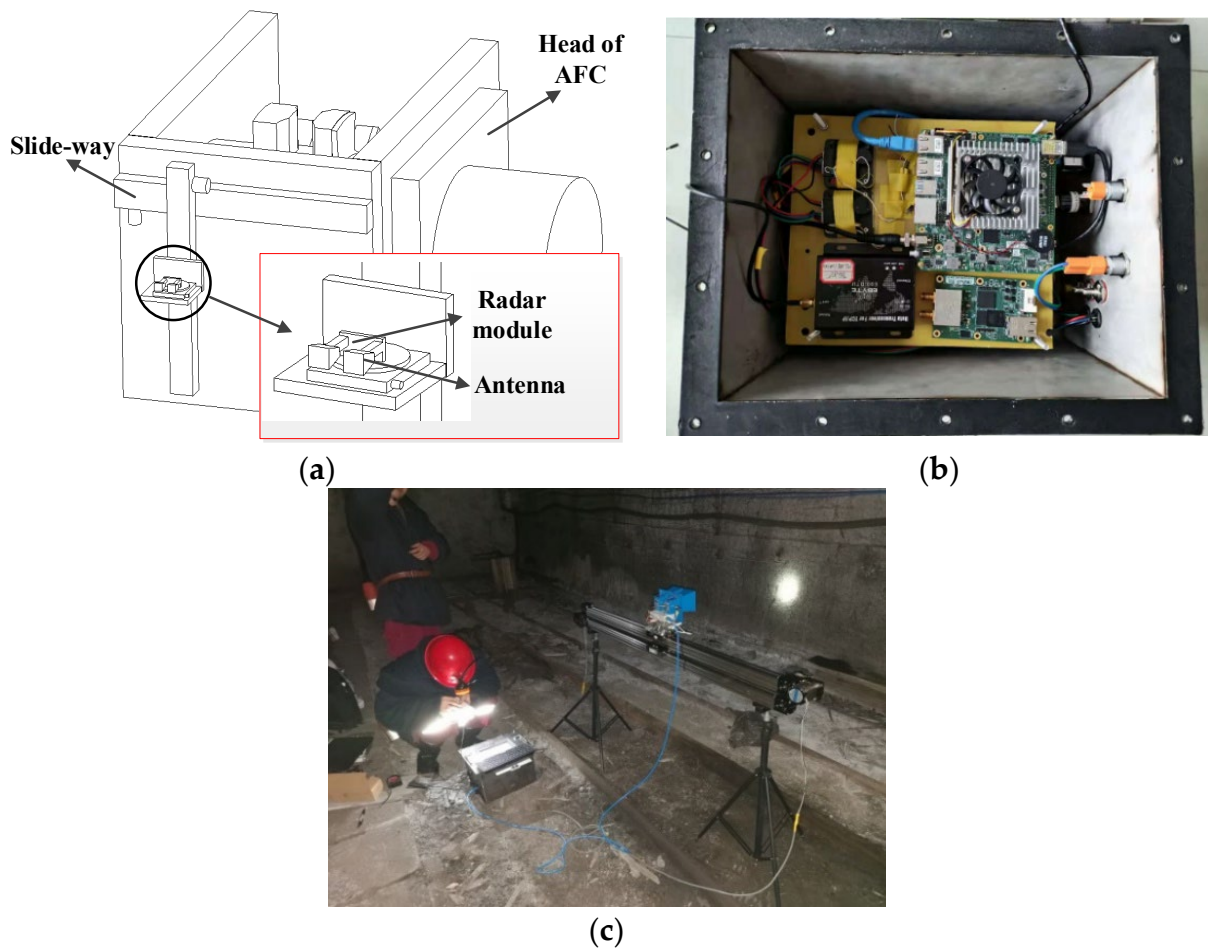


Figure 14. The diagram of (a) the measurement principle, (b) the measurement device, and (c) a field test in an underground coal mine [32].

3.3. The Backward Calibration of Shearer Trajectory

According to the measured retreat and creep displacements outlined in Section 3.2, the start and end points of each cutting cycle can be determined. In the LASC, the minimum-variance fixed-interval smoothing (MFS) algorithm was applied to correct the shearer trajectory backwardly when the shearer remains stationary at the end of the longwall face [33]. In fixed-interval smoothing, the estimation of the current state is based on the utilization of the measurement data from both before and after the current time within the interval. Smoothing is an off-line processing algorithm. Compared with filtering, smoothing can provide better estimation accuracy with the double computation load. The minimum-variance fixed-interval smoothing algorithm is briefly expressed as follows.

Suppose that the system satisfies the state equation and observation equation as Equations (1) and (2).

$$X_{k+1} = F_k X_k + B_k W_k \tag{1}$$

where X_k is the state vector, F_k is the state transition matrix, B_k is the noise transition matrix, and W_k is the state noise whose covariance is Q_k .

$$Z_k = H_k X_k + V_k \tag{2}$$

where Z_k is the observation vector, H_k is the observation transition matrix, and V_k is the observation noise whose covariance is R_k .

There are N sample data in the system. The smoothing algorithm has two steps. Step 1: calculating (3) from $k = 0$ to $k = N$ to obtain α_k . Step 2: calculating (4) from $k = N$ to $k = 0$ to acquire β_k under the known α_k from (3).

$$\begin{bmatrix} X_{k+1} \\ \alpha_k \end{bmatrix} = \begin{bmatrix} F_k - K_k H_k & K_k \\ -H_k (H_k P_{k-1} H_k^T + R_k)^{-1/2} & (H_k P_{k-1} H_k^T + R_k)^{-1/2} \end{bmatrix} \begin{bmatrix} X_k \\ Z_k \end{bmatrix}, X_0 = 0 \quad (3)$$

$$\begin{bmatrix} Y_{k-1} \\ \beta_k \end{bmatrix} = \begin{bmatrix} F_k^T - H_k^T K_k^T & H_k^T (H_k P_{k-1} H_k^T + R_k)^{-1/2} \\ -K_k^T & (H_k P_{k-1} H_k^T + R_k)^{-1/2} \end{bmatrix} \begin{bmatrix} Y_k \\ \alpha_k \end{bmatrix}, Y_N = 0 \quad (4)$$

where K_k is the gain, which can be given as (5), and P_k is the mean square of the system, which is updated as (6).

$$K_k = F_k P_{k-1} H_k^T (H_k P_{k-1} H_k^T + R_k)^{-1} \quad (5)$$

$$P_k = H_k P_{k-1} H_k^T - K_k (H_k P_{k-1} H_k^T + R_k) K_k^T + B_k Q_k B_k^T \quad (6)$$

Therefore, the estimated output is expressed as

$$\hat{Z}_k = Z_k - R_k \beta_k \quad (7)$$

In CUMT, the authors of this paper proposed the global optimization model (GOM) for shearer trajectory through borrowing the simultaneous localization and mapping (SLAM) technology. The SLAM frame is divided into front-end and back-end procedures [34,35]. The front-end process acquires the environment information using a camera or lidar to realize the map construction. The back-end step is to realize the map optimization and obtain the estimated pose according to the constraint information from the loop closure. This step is generally implemented using g2o [36] and Ceres-solver [37]. The GOM is described in detail as follows.

The dead-reckoning algorithm is used to calculate the shearer position based on the INS and axial encoder as (8).

$$\begin{aligned} N_k &= N_{k-1} + v_k T \cos \varphi_k \cos \theta_k \\ E_k &= E_{k-1} + v_k T \sin \varphi_k \cos \theta_k \\ U_k &= U_{k-1} + v_k T \sin \theta_k \end{aligned} \quad (8)$$

where N_k , E_k , and U_k are the shearer measurement position in the north, east, and up; v_k is the shearer velocity provided by the axial encoder; T is the sampling period; and φ_k and θ_k are the heading and pitch angles measured by the INS. As introduced in Section 3.1, the heading drift error is much larger than the drift error of the pitch. Therefore, this paper only considers the heading drift error. According to the dead-reckoning algorithm, the position error caused by the heading drift in the north (ΔN_k) from $k - 1$ to k can be expressed as

$$\Delta N_k = v_k T \cos \varphi_k \cos \theta_k - v_k T \cos(\varphi_k + \Delta \varphi_k) \cos \theta_k \quad (9)$$

where $\Delta \varphi_k$ is the absolute drift error of heading angle at k time, which is the sum of relative drift error (e_k) in each sampling period as (10).

$$\Delta \varphi_k = \sum_{k=1}^k e_k \quad (10)$$

Expanding ΔN_k into a power series of $\Delta \varphi_k$ at $\Delta \varphi_k = 0$ yields

$$\Delta N_k \approx H_1 \Delta \varphi_k + \frac{1}{2} H_2 \Delta \varphi_k^2 + \frac{1}{6} H_3 \Delta \varphi_k^3 \quad (11)$$

where H_1, H_2 , and H_3 are coefficients found in (12).

$$\begin{aligned}
 H_1 &= \frac{d(\Delta N_k)}{d(\Delta \varphi_k)} = v_k T \sin(\varphi_k + \Delta \varphi_k) \cos \theta_k \\
 H_2 &= \frac{d^2(\Delta N_k)}{d(\Delta \varphi_k)^2} = v_k T \cos(\varphi_k + \Delta \varphi_k) \cos \theta_k \\
 H_3 &= \frac{d^3(\Delta N_k)}{d(\Delta \varphi_k)^3} = -v_k T \sin(\varphi_k + \Delta \varphi_k) \cos \theta_k
 \end{aligned}
 \tag{12}$$

Similarly, the position error caused by the heading drift in the east (ΔE_k) from $k - 1$ to k is given as (13).

$$\Delta E_k = v_k T \sin \varphi_k \cos \theta_k - v_k T \sin(\varphi_k + \Delta \varphi_k) \cos \theta_k
 \tag{13}$$

ΔE_k is expanded into a power series of $\Delta \varphi_k$ as

$$\Delta E_k \approx J_1 \Delta \varphi_k + \frac{1}{2} J_2 \Delta \varphi_k^2 + \frac{1}{6} J_3 \Delta \varphi_k^3
 \tag{14}$$

where

$$\begin{aligned}
 J_1 &= \frac{d(\Delta E_k)}{d(\Delta \varphi_k)} = -v_k T \cos(\varphi_k + \Delta \varphi_k) \cos \theta_k \\
 J_2 &= \frac{d^2(\Delta E_k)}{d(\Delta \varphi_k)^2} = v_k T \sin(\varphi_k + \Delta \varphi_k) \cos \theta_k \\
 J_3 &= \frac{d^3(\Delta E_k)}{d(\Delta \varphi_k)^3} = v_k T \cos(\varphi_k + \Delta \varphi_k) \cos \theta_k
 \end{aligned}
 \tag{15}$$

Based on the above analysis, the objective function $F(e_k)$ is defined as

$$F(e_k) = \left| \left(\sum_{k=1}^m \Delta N_k \right) - \Delta P_N \right| + \left| \left(\sum_{k=1}^m \Delta E_k \right) - \Delta P_E \right|
 \tag{16}$$

where m is the number of sampling periods in a cutting cycle, and ΔP_N and ΔP_E are specifically described as (17).

$$\begin{aligned}
 \Delta P_N &= (N_m - N_1) - (N_{end} - N_{start}) \\
 \Delta P_E &= (E_m - E_1) - (E_{end} - E_{start})
 \end{aligned}
 \tag{17}$$

where N_1 and E_1 are the measured position coordinates of the start point in the north and east, N_m and E_m are the measured position coordinates of the end point, N_{start} and E_{start} are the accuracy position coordinates of the start point, and N_{end} and E_{end} are the accuracy position coordinates of the end point. Therefore, the global optimization problem of shearer positioning trajectory is reformulated as solving the minimum value of the objective function $F(e_k)$ as expressed in (18). In this study, the genetic algorithm (GA) is employed to compute this equation.

$$e_k^* = \underset{e_k}{\operatorname{argmin}} F(e_k)
 \tag{18}$$

The corrected heading angle is obtained via (19), which is used to obtain the shearer optimization trajectory with the dead-reckoning algorithm.

$$\varphi_k^* = \varphi_k + \sum_{k=1}^k e_k^*
 \tag{19}$$

In order to compare the performance of MFS and the GOM, an experiment was carried out as shown in Figure 15. The INS was installed at the center location of the mobile platform, and the axial encoder was connected to the wheel of mobile platform. At the same time, a Global Positioning System–Real-Time Kinematic (GPS-RTK) mobile station was installed above the INS, while the GPS-RTK base station was securely fixed on a predetermined location with known coordinates. The measurement trajectory of the base station was used to evaluate the positioning accuracy of the mobile platform. Additionally, it provided the position coordinates of the start point and end point for each cutting cycle. GPS-RTK height measurement exhibited an accuracy of less than 15 mm, while plane measurement demonstrated an accuracy of less than 8 mm. The mobile platform simulated four cutting cycles at a velocity of 0.1–0.2 m/s, and each cutting cycle covered a distance of about 100 m. The calculation period is set as 0.5 s. There were 2013, 2182, 2309, and 2047 sampling data during four cutting cycles, respectively. Figure 16 shows the comparison between GPS-RTK trajectory and shearer trajectories without processing, with MFS, and with GOM. It was evident that the trajectories with MFS and the GOM exhibited a higher degree of proximity to the RTK trajectory in comparison to the unprocessed trajectory. The position error in the north and east during each cutting cycle were calculated as described in Figures 17–20. For both the north and the east, the absolute values of position error with MFS first increased and then decreased. However, there was no such trend in position error with the GOM, which indicated that the GOM could restrain the heading drift well. The maximum position error during four cutting cycles with MFS and the GOM are listed in Table 1. The mean errors with MFS in the north and east were 0.1551 m and 0.1920 m, while the mean errors with the GOM were 0.0634 m and 0.0786 m, respectively. Table 2 shows the recorded duration with MFS and the GOM for four cutting cycles. In the GOM, the population size was 20 individuals, and the number of generations was set to 100. It was easily observed that the GOM took much more time than MFS. In brief, MFS had an advantage in terms of computation load, while the GOM achieved excellent accuracy.

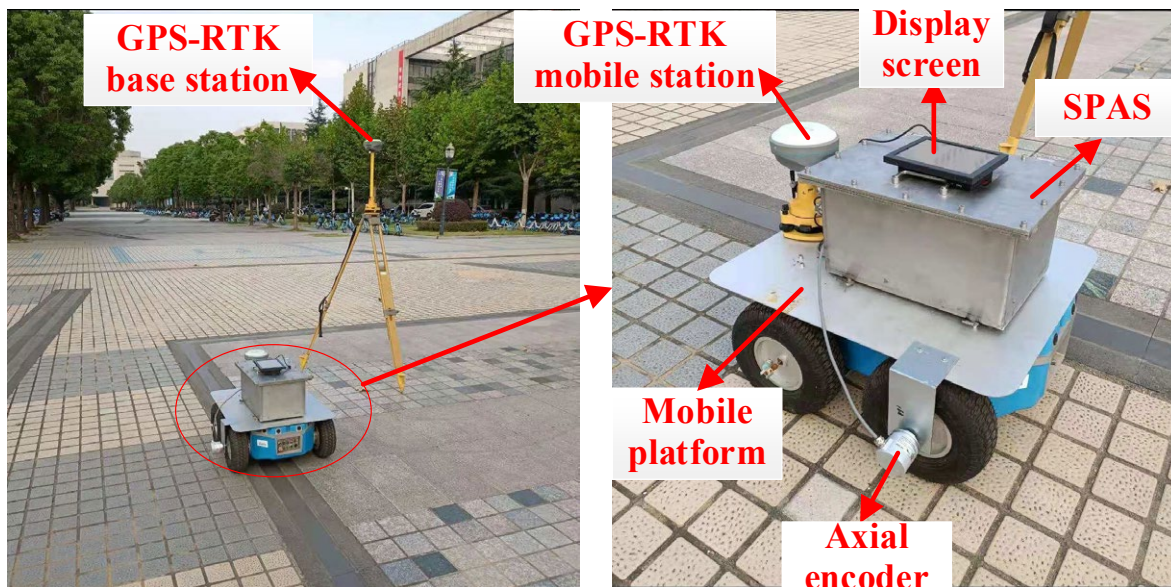


Figure 15. The diagram of the experiment site and device.

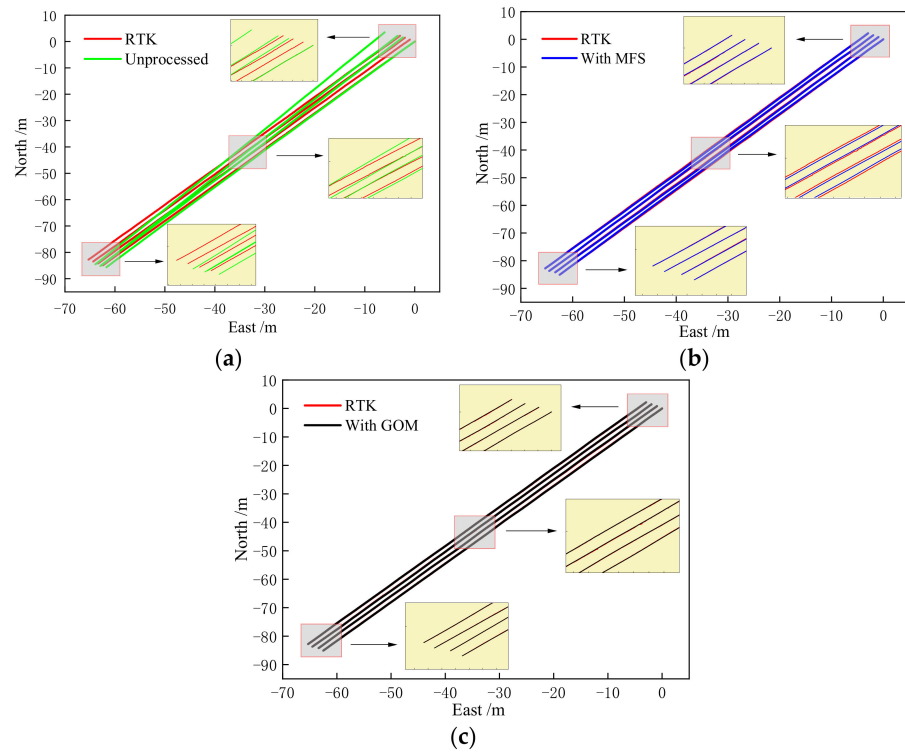


Figure 16. Comparison between RTK trajectory and shearer trajectory: (a) shearer trajectory without processing, (b) shearer trajectory with MFS, and (c) shearer trajectory with GOM.

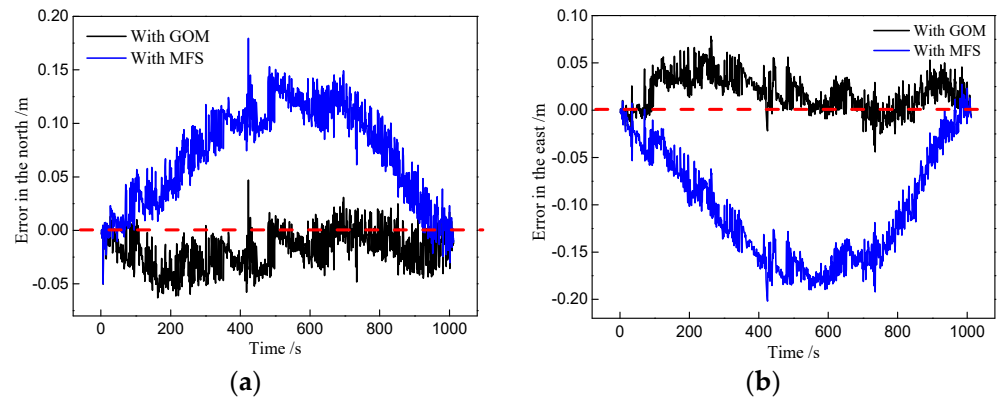


Figure 17. The position error of the first cutting cycle in the (a) north and (b) east.

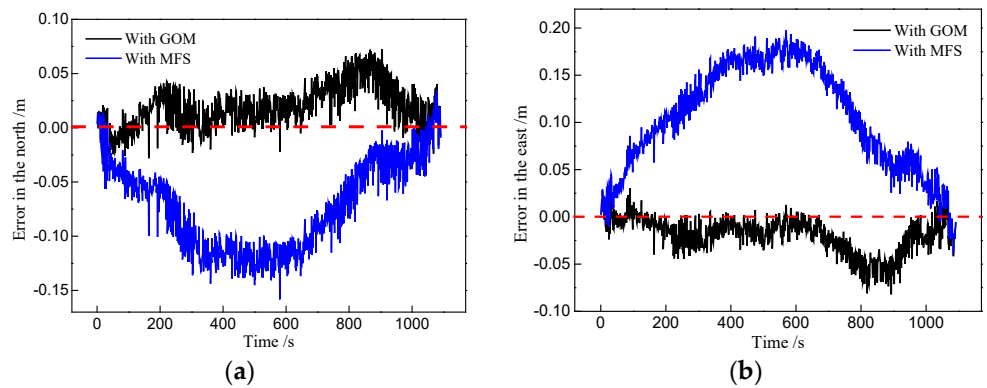


Figure 18. The position error of the second cutting cycle in the (a) north and (b) east.

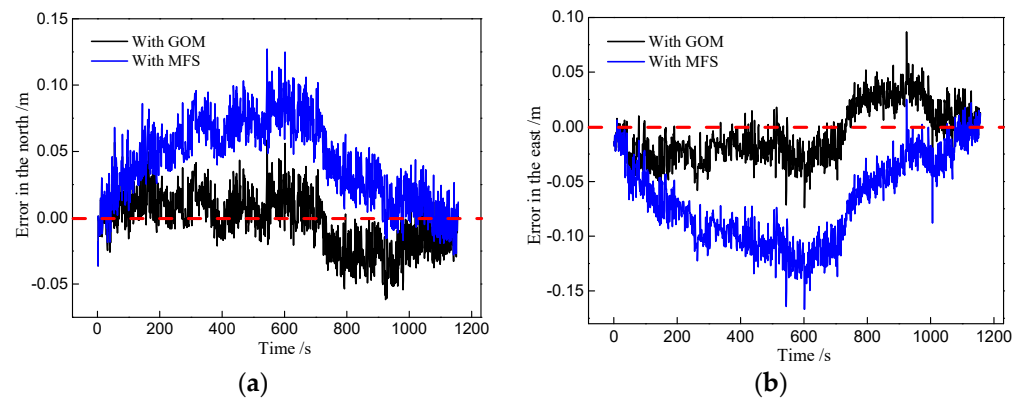


Figure 19. The position error of the third cutting cycle in the (a) north and (b) east.

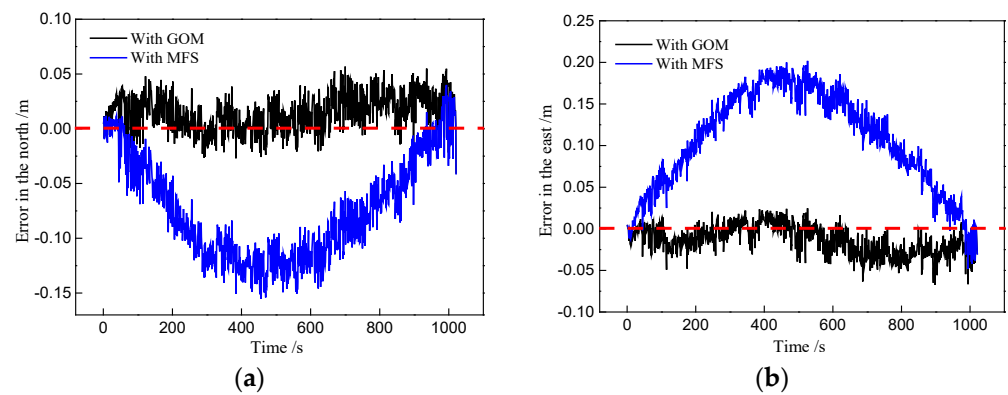


Figure 20. The position error of the fourth cutting cycle in the (a) north and (b) east.

Table 1. The maximum position error (m) with MFS and the GOM during four cutting cycles.

Cutting Cycles	MFS		GOM	
	North	East	North	East
First	0.1795	0.2017	0.0631	0.0781
Second	0.1583	0.1975	0.0725	0.0820
Third	0.1272	0.1669	0.0617	0.0868
Fourth	0.1553	0.2018	0.0562	0.0673
Mean error	0.1551	0.1920	0.0634	0.0786

Table 2. The elapsed time (s) with MFS and the GOM during four cutting cycles.

Cutting Cycles	MFS	GOM
First	1.6942	202.5673
Second	1.8814	260.5997
Third	1.9999	293.0323
Fourth	1.7098	229.5243

4. Discussion

The industrial experiments in acquiring the 3D shearer position conducted by the LASC and CUMT have all demonstrated satisfactory performance, which indicates that integrated navigation using the INS and axial encoder is an effective approach for addressing the shearer automation positioning. One difference is that the LASC uses the IXSEA PHINS INS, while the Spatial FOG INS is adopted in CUMT. The cost of the Spatial FOG INS is only one fifth that of the IXSEA PHINS INS. The same performance as a military INS

is achieved because the authors of this paper develop a series of error reduction algorithms through fully analyzing the longwall mining method as introduced in Section 3.1.

For the measurement of longwall retreat and creep displacements, the proposed SAR imaging method has two advantages. First, the propagation of radar signals in underground mines is hardly affected by the presence of dust and moisture. Second, this method is an autonomous measurement technology which does not depend on external information. This method images the bolt-plates fixed in the roadway wall as the targets due to their higher reflective intensity. Although the surrounding objects may affect the imaging result, this method still has strong robustness from the final result of image registration.

Compared with MFS, the GOM has better performance in backward-correcting the shearer trajectory. Because it needs to iterate to find the optimal value with GA, the GOM has more working time. In the experiment, there are about 2000 data in each cutting cycle, which takes 4 min for the GOM to complete. If a typical longwall face is 300 m long, the running time of the GOM (more than 12 min) will be greater than the time when the shearer is stationary at the end of the longwall face, which limits its practical application. Therefore, it is an urgent problem to find a backward calibration method with high precision and small calculation load.

5. Conclusions

In order to realize the automatic and accurate positioning of shearers in underground mines, the LASC and CUMT adopt the same technical route, which includes three key technologies, the shearer inertial navigation system, the measurement of longwall retreat and creep displacements, and the backward calibration of the shearer trajectory. With INS as the core unit, the LASC and CUMT develop SPMS and SPAS, respectively. At the end of a longwall face, a scanning laser and a FMR 250 microwave radar are used to measure the retreat and creep displacements, and a UWB radar is adopted in CUMT to measure those two displacements with consideration of the complex environment with dust and water vapor. In order to perform backward calibration of the shearer trajectory, MFS and the GOM are proposed by the LASC and CUMT, respectively. Comparisons are made through the experiment, which shows that MFS has better performance in computation load, while the GOM achieves satisfactory accuracy. Next, a high efficiency and accurate algorithm to back-correct the shearer trajectory is our research goal.

Author Contributions: Conceptualization, W.D., S.W. (Shijia Wang), and S.W. (Shibo Wang); methodology, W.D. and S.W. (Shijia Wang); software, W.D. and S.W. (Shijia Wang); validation, S.W. (Shibo Wang); formal analysis, W.D.; investigation, W.D. and S.W. (Shijia Wang); resources, S.W. (Shibo Wang); data curation, W.D. and S.W. (Shijia Wang); writing—original draft preparation, W.D. and S.W. (Shijia Wang); writing—review and editing, S.W. (Shijia Wang); visualization, W.D. and S.W. (Shijia Wang); supervision, S.W. (Shibo Wang); project administration, S.W. (Shibo Wang); funding acquisition, S.W. (Shibo Wang). All authors have read and agreed to the published version of the manuscript.

Funding: This research was funded by the National Natural Science Foundation of China, Grant Nos. 52304180 and Nos. 51874279, the Program of Ministry of Industry and Information Technology (TC220A04W-1,167), the Shanxi Key Research and Development Program of China (2021020101003) and the Priority Academic Program Development of Jiangsu Higher Education Institutions (PAPD).

Institutional Review Board Statement: Not applicable.

Informed Consent Statement: Not applicable.

Data Availability Statement: The data presented in this study are available on request from the corresponding author. The data are not publicly available due to privacy .

Conflicts of Interest: The authors declare no conflict of interest.

References

1. Singh, R.D. *Principles and Practices of Modern Coal Mining*; New Age International: New Delhi, India, 2004.
2. Van Duin, S.; Meers, L.; Donnelly, P.; Oxley, I. Automated bolting and meshing on a continuous miner for roadway development. *Int. J. Min. Sci. Technol.* **2013**, *23*, 55–61. [[CrossRef](#)]
3. Ge, S. Key technology of intelligent coal mining equipment. *Coal Sci. Technol.* **2014**, *42*, 7–11. (In Chinese)
4. Yuan, L. Scientific conception of precision coal mining. *J. China Coal Soc.* **2017**, *42*, 1–7. (In Chinese)
5. Ralston, J.C.; Hargrave, C.O.; Dunn, M.T. Longwall automation: Trends, challenges and opportunities. *Int. J. Min. Sci. Technol.* **2017**, *27*, 733–739. [[CrossRef](#)]
6. Wang, J.; Huang, Z. The Recent Technological Development of Intelligent Mining in China. *Engineering* **2017**, *3*, 439–444. [[CrossRef](#)]
7. Ralston, J.; Reid, D.; Hargrave, C.; Hainsworth, D. Sensing for advancing mining automation capability: A review of underground automation technology development. *Int. J. Min. Sci. Technol.* **2014**, *24*, 305–310. [[CrossRef](#)]
8. Reid, D.C.; Hainsworth, D.W.; Ralston, J.C.; McPhee, R.J. Shearer guidance: A major advance in longwall mining. In Proceedings of the 4th International Conference on Field and Service Robotics, Lake Yamanaka, Japan, 14–16 July 2003; Springer: Berlin/Heidelberg, Germany, 2003; pp. 469–476.
9. Available online: <http://www.lascautomation.com/lasc-compliance.html> (accessed on 18 February 2008).
10. Ge, S.; Su, Z.; Li, A.; Wang, S.; Hao, S.; Liu, W.; Meng, L. Study on the positioning and orientation of a shearer based on geographic information system. *J. China Coal Soc.* **2015**, *40*, 2503–2508.
11. Wang, S.; Wang, S. Improving the Shearer Positioning Accuracy Using the Shearer Motion Constraints in Longwall Panels. *IEEE Access* **2020**, *8*, 52466–52474. [[CrossRef](#)]
12. Zhang, Q.Q.; Zhao, L.; Zhou, J.H.; Wang, B.H.; Zhang, Y.P. A real-time airborne terrain aided inertial navigation system and its performance analysis. *Adv. Space Res.* **2017**, *60*, 2751–2762. [[CrossRef](#)]
13. Zhang, C.; Guo, C.; Zhang, D. Ship navigation via GPS/IMU/LOG integration using adaptive fission particle filter. *Ocean. Eng.* **2018**, *156*, 435–445. [[CrossRef](#)]
14. Huang, H.; Chen, X.; Zhang, B.; Wang, J. High accuracy navigation information estimation for inertial system using the multi-model EKF fusing Adams explicit formula applied to underwater gliders. *ISA Trans.* **2017**, *66*, 414–424. [[CrossRef](#)] [[PubMed](#)]
15. Titterton, D.; Weston, J.L.; Weston, J. *Strapdown Inertial Navigation Technology*; IET: Stevenage, UK, 2004.
16. Wang, X. *The Foundation of Inertial Navigation*; Northwestern Polytechnical University Press Co., Ltd.: Xi'an, China, 2012. (In Chinese)
17. Reid, D.C.; Dunn, M.T.; Reid, P.B.; Ralston, J.C. A practical inertial navigation solution for continuous miner automation. In Proceedings of the 12th Coal Operators' Conference, University of Wollongong & the Australasian Institute of Mining and Metallurgy, Perth, Australia, 8–10 October 2012; pp. 114–119. Available online: <https://ro.uow.edu.au/coal/398/> (accessed on 16 February 2012).
18. Dunn, M.T.; Thompson, J.P.; Reid, P.B.; Reid, D.C. High accuracy inertial navigation for underground mining machinery. In Proceedings of the 2012 IEEE International Conference on Automation Science and Engineering (CASE), Seoul, Republic of Korea, 20–24 August 2012; pp. 1179–1183.
19. Dunn, M.; Reid, D.; Ralston, J. Control of automated mining machinery using aided inertial navigation. In Proceedings of the Machine Vision and Mechatronics in Practice, Toowoomba, Australia, 7–9 December 2015; Springer: Berlin/Germany, Germany, 2015; pp. 1–9.
20. Reid, D.; Ralston, J.; Dunn, M.; Hainsworth, D. Longwall Shearer Automation: From Research to Reality. In Proceedings of the Machine Vision and Mechatronics in Practice, Toowoomba, Australia, 7–9 December 2015; Springer: Berlin/Heidelberg, Germany, 2015.
21. Ralston, J.C.; Reid, D.C.; Dunn, M.T.; Hainsworth, D.W. Longwall automation: Delivering enabling technology to achieve safer and more productive underground mining. *Int. J. Min. Sci. Technol.* **2015**, *23*, 47–53. [[CrossRef](#)]
22. Hao, S.; Li, A.; Wang, S.; Ge, Z.; Zhang, Z.; Ge, S. Effects of shearer inertial navigation installation noncoincidence on shearer positioning error. *J. China Coal Soc.* **2015**, *40*, 1963–1968. (In Chinese)
23. Zhang, B.; Wang, S.; Ge, S. Effects of initial alignment error and installation noncoincidence on the shearer positioning accuracy and calibration method. *J. China Coal Soc.* **2017**, *42*, 789–795. (In Chinese)
24. Li, A. Research on Shearer Absolute Positioning and Attitude Technology in Mining Area. Master's Thesis, China University of Mining and Technology, Xuzhou, China, 2015. (In Chinese).
25. Zhang, B. Research on Dynamic Accurate Positioning Method of Shearer. Master's Thesis, China University of Mining and Technology, Xuzhou, China, 2017. (In Chinese).
26. Wang, S.; Wang, S.; Zhang, B.; Ge, S. Dynamic zero-velocity update technology to shearer inertial navigation positioning. *J. China Coal Soc.* **2018**, *43*, 578–583.
27. Wang, S.; Zhang, B.; Wang, S.; Ge, S. Dynamic precise positioning method of shearer based on closing path optimal estimation model. *IEEE Trans. Autom. Sci. Eng.* **2019**, *16*, 1468–1475.
28. Hao, S. Research on Navigation and Self-Adaptive Cutting Control Technology of Shearer Based on Coal Seam Structure. Ph.D. Thesis, China University of Mining and Technology, Xuzhou, China, 2017.

29. Hargrave, C.O.; James, C.A.; Ralston, J.C. Infrastructure-based localisation of automated coal mining equipment. *Int. J. Coal Sci. Technol.* **2017**, *4*, 252–261. [[CrossRef](#)]
30. Hargrave, C.O.; Shuley, N.V.; Ralston, J.C.; Hainsworth, D.W. Radar level sensor for longwall creep and retreat measurement. In Proceedings of the 2007 IEEE Industry Applications Annual Meeting, New Orleans, LA, USA, 23–27 September 2007; pp. 2102–2109.
31. Hargrave, C.; Clarkson, I.V.L.; Lui, H.S. Radar waypoint navigator for underground mining. In Proceedings of the 8th European Conference on Antennas and Propagation (EuCAP 2014), The Hague, The Netherlands, 6–11 April 2014; pp. 3587–3591.
32. Wang, S.; Wang, S. UWB Radar Imaging Method for the Longwall Retreat and Creep Displacements Measurement in Underground Coal Mine. *IEEE Trans. Autom. Sci. Eng.* **2023**. *early access*. [[CrossRef](#)]
33. Einicke, G.A.; Ralston, J.C.; Hargrave, C.O.; Reid, D.C.; Hainsworth, D.W. Longwall mining automation an application of minimum-variance smoothing. *IEEE Control Syst.* **2008**, *28*, 28–37. [[CrossRef](#)]
34. Huang, S.; Dissanayake, G. A critique of current developments in simultaneous localization and mapping. *Int. J. Adv. Robot. Syst.* **2016**, *13*, 1729881416669482. [[CrossRef](#)]
35. Chen, C.; Zhu, H.; Li, M.; You, S. A Review of Visual-Inertial Simultaneous Localization and Mapping from Filtering-Based and Optimization-Based Perspectives. *Robotics* **2018**, *7*, 45. [[CrossRef](#)]
36. Kümmerle, R.; Grisetti, G.; Strasdat, H.; Konolige, K.; Burgard, W. G2o: A general framework for graph optimization. In Proceedings of the IEEE International Conference on Robotics and Automation, Shanghai, China, 9–13 May 2011; pp. 3607–3613.
37. Hess, W.; Kohler, D.; Rapp, H.; Andor, D. Real-time loop closure in 2D LIDAR SLAM. In Proceedings of the IEEE International Conference on Robotics and Automation, Stockholm, Sweden, 16–21 May 2016; pp. 1271–1278.

Disclaimer/Publisher’s Note: The statements, opinions and data contained in all publications are solely those of the individual author(s) and contributor(s) and not of MDPI and/or the editor(s). MDPI and/or the editor(s) disclaim responsibility for any injury to people or property resulting from any ideas, methods, instructions or products referred to in the content.